Journal of Power Sources 188 (2009) 163–169

Contents lists available at ScienceDirect

Journal of Power Sources

journal homepage: www.elsevier.com/locate/jpowsour

The critical pressure drop for the purge process in the anode of a fuel cell

Xiao Yu[a,b], Ming Pingwen[c,*], Hou Ming[a], Yi Baolian[a], Zhi-Gang Shao[a]

[a] Dalian Institute of Chemical Physics, Dalian 116023, Liaoning, China
[b] Chinese Academy of Sciences, Dalian 116023, Liaoning, China
[c] Dalian Sunrise Power Co., Ltd., Dalian 116025, Liaoning, China

ARTICLE INFO

Article history:
Received 21 September 2008
Received in revised form
19 November 2008
Accepted 19 November 2008
Available online 3 December 2008

Keywords:
Fuel cell
Water removal
Two-phase flow
Mini-channel
Anode
Purge

ABSTRACT

Purge operation is an effective way to remove the accumulated liquid water in the anode of proton exchange membrane fuel cells (PEMFCs). This paper studies the phenomenon of the two-phase flow as well as the pressure drop fluctuation inside the flow field of a single cell during the purge process. The flow patterns are identified as intermittent purge and annular purge, and the two purge processes are contrastively analyzed and discussed. The intermittent purge greatly affects the fuel cell performance and thus it is not suitable for the in situ application. The annular purge process requires a higher pressure drop, and the critical pressure drop is calculated from the annular purge model. Furthermore, this value is quantitatively analyzed and validated by experiments. The results show that the annular purge is appropriate for removing liquid water out of the anode in the fuel cell.

1. Introduction

Proton exchange membrane fuel cells (PEMFCs) are regarded as the most promising energy conversion systems for transportation and stationary applications in the future [1]. PEMFC technologies, which have been applied to vehicles, have attracted increasing attention because of their high energy conversion efficiency and zero emissions.

Water management in PEMFCs is a key issue for obtaining stable performance [2,3], and how to remove the accumulated water in the anode effectively is of paramount importance for fuel cell operation. The excess liquid water resulting from back diffusion can block the anode channel and cause the unstable performance of the cell [4], thus, the water is usually removed by purge process in the practical application. To analyze the purge process involved in such situations, two-phase flow in the anode should be taken into account [5]. The characteristics in the mini-channels of the fuel cell flow field are different with those in macro-channels. Among the numerous differences, the surface tension may take the main effect instead of gravity or bulk forces [6–8]. Many well-known correlations related to pressure drop in channels were put forward previously [9–11]; in macro-channels, these models work well, while further research work should be done to determine whether they are applicable for fuel cell channels, whose cross-section is rectangular in the mini-range (about 1 mm). Because the flow distribution is non-uniform in the multi-parallel channel [12], and the water droplets appear randomly in the flow field, we first concentrate on one channel to discuss the two-phase interactions.

On the basis of the background above, a transparent fuel cell is designed to observe the flow patterns, especially during the purge process when the hydrogen flows upward. Because this direction is easy for water accumulation, so it is the worst situation for practical application. Then the two-phase flow pattern at purge is identified in situ and the total pressure drops are recorded with the flow rates. By analyzing the signal of pressure drop fluctuation, the typical flow pattern and the drainage effect are reflected. Compared with the model prediction, the critical pressure drop for annular purge in this single channel is discussed in macroscopic view.

2. Experimental

2.1. Specifications of the test facility

To investigate the two-phase flow pattern in the anode channel, a simple transparent cell, which has a single straight gas flow channel (GFC), is set up as shown in Fig. 1. The transparent plates are made of polymethyl methacrylate (PMMA), while the flow plate (also the current collector) is made of SUS306, which is silvered to reduce the contact resistance. The operation temperature of the cell is controlled by the circulating water. The GFC rectangu-

* Corresponding author. Tel.: +86 411 84617012; fax: +86 411 84753456.
E-mail address: pwming@dicp.ac.cn (M. Pingwen).

0378-7753/$ – see front matter © 2008 Elsevier B.V. All rights reserved.
doi:10.1016/j.jpowsour.2008.11.105

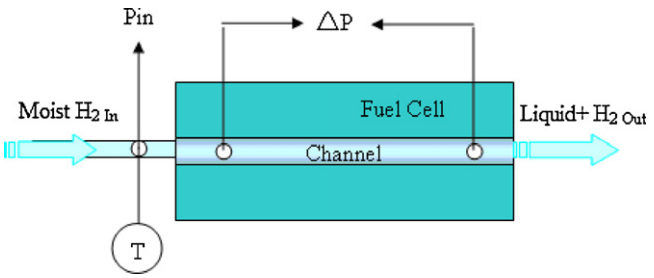

Fig. 1. Top view of the anode with the transparent plate.

lar cross-section is 0.7 mm high and 1.3 mm wide. The test region is chosen 300 mm long and 29 mm away from the inlet or outlet to reduce turbulence and non-homogenous effects. Two pressure transducers are used for pressure measurements over the range of 0–3 kPa (STD110 Honeywell) and 0–20 kPa (STD930 Honeywell) with 0.065% full-scale accuracy for both. The inlet pressure and pressure difference are recorded 10 times during 1 s, and these data along with the flow rates, temperature and voltages under the different currents are stored in computer. In our experiments, the fuel cell consists of a membrane electrode assembly (MEA) with Nafion 1035 membrane and catalyst loading of 0.3 mg cm^{-2} on each electrode. Toray carbon papers (TGP-H-060), 20 wt %, wet proofed with polytetrafluoroethylene (PTFE) are employed as gas diffusion layer (GDL) along with microporous layers (MPL). The active area of MEA is 4.55 cm^2 (1.3 mm × 350 mm).

2.2. Water accumulation and the two purge processes

Because water accumulation in the anode is a long and complicated process, the main purpose of this paper is to observe the purge process in the anode GFC, especially for the upflow under the given conditions. In order to accelerate the liquid water accumulation, the moist hydrogen is used. The relative humidity of the gas after passing the humidifier is 100%, which is indicated by the use of Vaisala's HMP363 hygrometer. The relative operation conditions in Fig. 2 are described as follows: the cell temperature was controlled to be 50 °C, while the humidifiers were kept at 60 °C. Current densities used in this study were step-changed, from 0.2, 0.6, 0.8, 1.0, and 1.2 A cm^{-2} by turns, while the volume velocity of hydrogen was maintained at 96 sccm and the air velocity was 228 sccm. Thus, the corresponding hydrogen stoichiometric ratios were 15.1, 5.0, 3.8, 3.0 and 2.5 lasting for every 10 min. The response voltages were captured by Arbin instrument every 2 s (see Fig. 2(b)). The purge process, which had a sharp peak value, appeared under the above conditions. Comparing with the response voltages simultaneously, the effects of the water behavior on cell voltage were shown in Fig. 2(c).

2.2.1. Intermittent purge process

The purging process was captured by CCD camera as shown in Fig. 3. Sometime the liquid water blocked the channel (Fig. 3(a), $t = 0$ s), which usually happens after the discharging process with higher stoichiometric ratio. That is because more hydrogen was consumed during discharging process with lower stoichiometric ratio and then, more liquid water appeared. When the stoichiometric ratio reached higher, the hydrogen flow would cause the liquid films more disturbing, thus, it would block the channel easily. Then the liquid column moved upwards with growing or just 'hung' in the flow field (Fig. 3(b), $t = 0.5$ s), which could cause the pressure increased if the gas continued to flow in. When the increased pressure difference between the column ends grew big enough to overcome the bulk and frictional force, the liquid column would move again (Fig. 3(c), $t = 19.5$ s). At the same time, some of the films still adhered to the wall and stayed at the GFC. At last, some of the

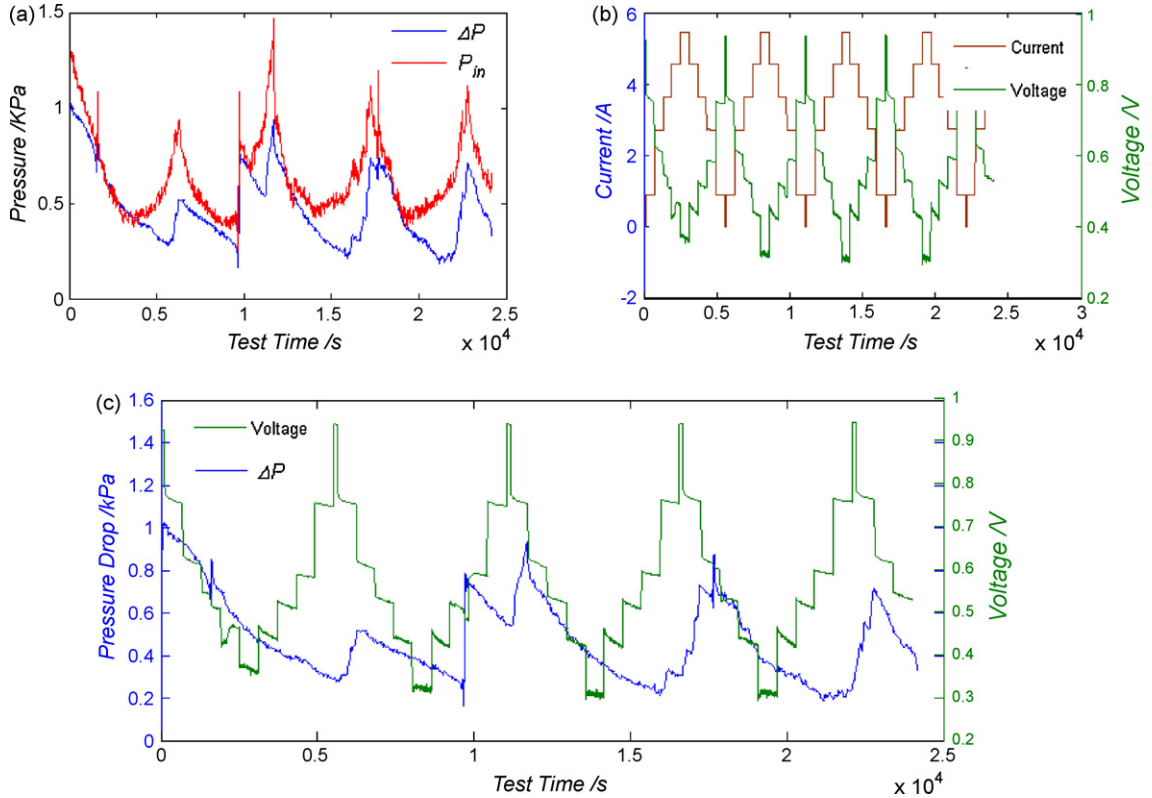

Fig. 2. The effect of the water behavior on cell voltage under practical conditions: (a) the fluctuation of the pressure at the inlet and the corresponding pressure drop, (b) the setting currents and the response voltages, and (c) changes of the voltages of the cell and the pressure drops in the channel.

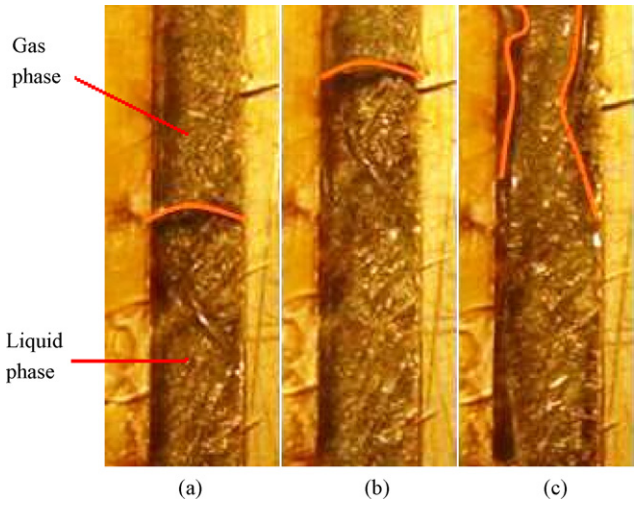

Fig. 3. The intermittent purge process in the anode GFC: (a) $t = 0$ s, (b) $t = 0.5$ s, and (c) $t = 19.5$ s.

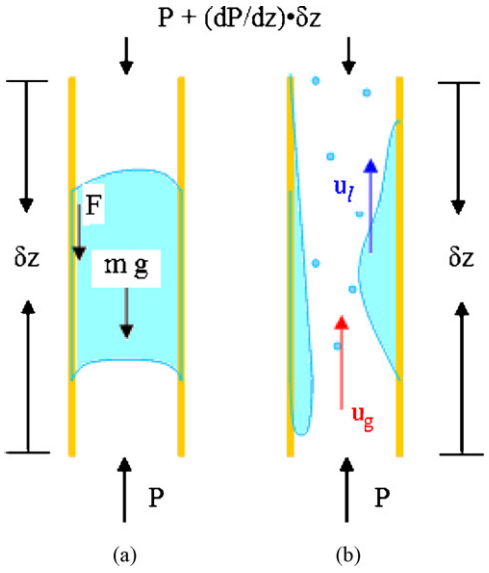

Fig. 4. The schematic diagrams of the two purge process: (a) intermittent purge and (b) annular purge.

accumulated water might be removed from the fuel cell by the intermittent flow and this process was called the intermittent purge. In addition, the ends of the liquid column were given uneven forces during the intermittent purge, and the column might be passed through by the gas phase. Thus, the new liquid drops or films would adhere to the GFC surface again, and led to higher pressure drop. In fact, most of the accumulated water would stay at the channel during the intermittent purge process, especially in the upflow. It may lead to localized fuel starvation and consequently performance degradation of the fuel cell. Next, we will discuss another purge process, the annular purge process.

2.2.2. Annular purge process

When a stronger pulse flow happens, the liquid films may become very disturbed with large waves. Some of the liquid drops are propelled by the gas flow above the liquid films. There are a large number of liquid drops formed in the chaotic flow, which nearly move upwards. This pressure difference is called the critical pressure drop. If the pressure drop is higher, more and more liquid drops move up, and then the co-current annular flow is formed. We call it annular purge. Comparing the schematic diagrams of intermittent and annular purge process (see Fig. 4), the liquid phase cannot block the channel in the annular purge process. Usually, a hydrophilic channel side-wall with a hydrophobic MEA surface is applied, and then most liquid water accumulates on the surface of GFC [13]. If the water can be removed by the annular purge time and again, it will avoid water accumulation on the MEA surface, less affecting the mass transfer in the GDL.

In summary, the intermittent purge, which will increase the operation instability and shorten the cell life, should be avoided; while the annular purge needs higher pressure drop to gain enough speed to remove the liquid water, thus, this critical pressure drop should be found out.

3. Annular purge model

3.1. The correlations under the critical condition

We know that liquid water is easy to accumulate in the upflow, and it needs higher pressure drop to purge the liquid out of the cell than other directions. Thus, we mainly focus on this upflow to solve the worst situation. As we have described the critical condition in Section 2.2.2, the two-phase flow will turn to chaotic flow when there is enough pressure drop between the ends of the channel. It can be applied to a separated flow system. The normally used methods of correlations are of two types: the Wallis type [14] and the Kutatelaze number correlation [15]. However, better overall results are obtained with an optimized correlation by McQuillan et al. [16]. Here we adopt this method as follows:

$$\mathrm{Ku} = 0.286\mathrm{Bo}^{0.26}\mathrm{Fr}^{-0.22}\left[1 + \frac{\mu_l}{\mu_w}\right]^{-0.18} \quad (1)$$

where

$$\text{Ku is the Kutateladze number} = \frac{V_g \rho_g^{1/2}}{[g\sigma(\rho_l - \rho_g)]^{1/4}} \quad (2)$$

$$\text{Bo is the Bond number} = \frac{D_e^2 g(\rho_l - \rho_g)}{\sigma} \quad (3)$$

$$\text{Fr is the Froude number} = V_l \frac{\pi}{4}\left[\frac{g(\rho_l - \rho_g)}{\sigma}\right]^{1/4} \quad (4)$$

μ_l is the liquid viscosity (Pa s); and μ_w is the water viscosity (at room temperature) = 10^{-3} Pa s. D_e is the equivalent diameter of the GFC (m). Therefore, if we get the gas superficial velocity V_g (m s^{-1}), the liquid superficial velocity V_l (m s^{-1}) will be deduced under the critical condition.

3.2. Pressure drops in two-phase flow

Based on the relationship of V_g and V_l above, the critical pressure drops can be calculated with the two-phase separated flow model [16,17]. As for the two-phase flow, the total pressure drop is divided into three components, and can be expressed as the frictional, gravitational, and momentum gradients.

$$-\left(\frac{dP}{dz}\right)_{\text{total}} = -\left(\frac{dP}{dz}\right)_{\text{frictional}} - \left(\frac{dP}{dz}\right)_{\text{gravitational}} - \left(\frac{dP}{dz}\right)_{\text{momentum}} \quad (6)$$

Next, every gradient will be discussed in detail:

(a) Firstly, it should be noted that the gravitational and momentum terms require a knowledge of the void fraction α, for which the

general equation is

$$\alpha = \left[1 + \left(S\frac{1-x}{x}\frac{\rho_g}{\rho_l}\right)\right]^{-1} \quad (7)$$

The velocity ratio u_g/u_l is often called the slip ratio S. For this separated flow, S is usually much greater than one, so that the hydrogen is moving faster than the liquid water in the anode of a fuel cell. Chisholm [18] produced a particularly simple correlation, which is

$$S = \left[1 - x\left(1 - \frac{\rho_l}{\rho_g}\right)\right]^{1/2} \quad (8)$$

Then the gravitational term can be expressed as

$$-\left(\frac{dP}{dz}\right)_{\text{gravitational}} = g[\alpha\rho_g + (1-\alpha)\rho_l]\sin\ \theta \quad (9)$$

where θ is the inclination angle of the flow direction to horizontal plane, and here it is 90°.

(b) Theory has, as yet, provided no help at all with the frictional term. Experiments about the system and correlations should be provided properly. Chisholm correlation is empirically derived from a vast pool of experimental data, and may be the available correlation for the frictional two-phase pressure gradient in the anode. It is written in terms of a two-phase multiplier:

$$\left(-\frac{dP}{dz}\right)_{\text{frictional}} = \left(-\frac{dP}{dz}\right)_l + C\left[\left(-\frac{dP}{dz}\right)_l\left(-\frac{dP}{dz}\right)_g\right]^{1/2} + \left(-\frac{dP}{dz}\right)_g \quad (10)$$

where $(-dP/dz)_l$ and $(-dP/dz)_g$ are the single-phase pressure gradients calculated using the actual phase flow rates for the two-phase flow. The magnitude of C, which was introduced by Chisholm, can be used to assess how important the specifically two-phase effects are in determining the two-phase frictional pressure drop. Because the velocities of the two phases are lower, and it should be noted that the laminar–laminar value for C is 5. The single-phase pressure gradient of the friction is usually expressed in terms of the friction coefficient C_f, which is defined by

$$C_f = \frac{\tau_i}{(1/2)\rho_i u_i^2} = \frac{\rho_i D_e(-dP/dz)_i}{2G_i^2} \quad (11)$$

where u_i is the actual velocity (m s^{-1}) and τ_i is the shear force (N m^{-2}) for i species. Hence,

$$-\left(\frac{dP}{dz}\right)_g = \frac{4C_f}{D_e}\frac{G_g^2}{2\rho_g} \quad (12)$$

$$-\left(\frac{dP}{dz}\right)_l = \frac{4C_f}{D_e}\frac{G_l^2}{2\rho_l} \quad (13)$$

here G_g and G_l are the mass flux of gas and liquid (kg m^{-2} s^{-1}) and C_f will be fitted in Section 4.1.

(c) When fuel cell is operating, the discharging progress will consume some hydrogen along the anode channel:

$$G_g(Z) = \left(1 - \frac{1}{\lambda}\frac{Z}{L}\right)G_g \quad (14)$$

where Z represents the distance from the inlet to the Z point along the channel (m) and λ is the stoichiometric ratio.

$$G_l(Z) = G_l + \frac{M_l}{M_g}\frac{Pw}{P - Pw}(G_g - G_g(Z)) \quad (15)$$

where Pw represents the saturated vapor pressure of water at a certain temperature (kPa).

$$G_{\text{total}}(Z) = G_l(Z) + G_g(Z) \quad (16)$$

Thus, the total pressure drop should be accumulated from the inlet to the outlet as follows:

$$-\int_0^L \left(\frac{dP}{dz}\right)_{\text{momentum}} dz = \left[G_{\text{total}}(z)^2\left(\frac{x(z)^2}{\alpha(z)\rho_g} + \frac{(1-x(z))^2}{(1-\alpha(z))\rho_l}\right)\right]_0^L \quad (17)$$

The algorithm for the calculation of the critical pressure drop is given in Appendix A and the specification of operating conditions and parameters are listed in Table 1.

Table 1
Specification of operating conditions and parameters.

Physical properties	Values
Length of the effective channel, L (m)	0.3
Equivalent diameter of the GFC, D_e (m)	9.1×10^{-4}
Cross-sectional area of the singel channel, A (m^2)	9.1×10^{-7}
Cell temperature (°C)	50
Hydrogen density, ρ_g (kg m^{-3}, 50 °C)	0.078
Water density, ρ_l (kg m^{-3}, 50 °C)	988.1
Hydrogen viscosity, μ_g (Pa s, 50 °C)	9.39×10^{-6}
Water viscosity, μ_l (Pa s, 50 °C)	54.94×10^{-5}
Water viscosity, μ_w (Pa s, 20 °C)	100.5×10^{-5}
Surface tension of water, σ (N m^{-1}, 50 °C)	67.7×10^{-3}
Saturated vapor pressure of water, Pw (kPa, 50 °C)	12.31
Inclination angle of the flow direction to horizontal plane, θ (°)	90

4. Result and discussions

4.1. The single-phase friction coefficient

Cai et al. [13] has investigated the effects of the hydrophilic/hydrophobic properties on water behavior inside a straight micro-channel by volume-of-fluid model. Then the local characteristics on the surface of GDL/GFC are clear, however, it fails to give the critical pressure drop for annular purge process in the macroscopic view. We consider the different surfaces of the channel as a whole, and then the friction coefficient (C_f) is used to generalize the effects of surface properties and channel configuration. The single-phase results give the friction coefficient as a function of Reynolds number (Re) and roughness (ε) of the channel. In general,

$$C_f = f\left(Re, \frac{\varepsilon}{d}\right) \quad (18)$$

Under our experimental conditions, the Reynolds numbers are usually less than 2000, thus, the friction coefficient (C_f) usually has inverse relation with Re. However, the flow hydrodynamics in this mini-channel are different from the ones in macro-range [19], and the friction coefficient need to be fitted by experiments with different fluids (see Fig. 5). In the upflow, the gravitational effect can be neglected for the hydrogen and air, but should be considered for the water. Thus, they nearly have the same slope when C_f is plotted against Re in log scale. It shows that the friction coefficient (C_f) can reflect the whole channel's characteristics independently. Then the equation of the fitted curve is shown as

$$C_f = \frac{33.8}{Re} \quad (19)$$

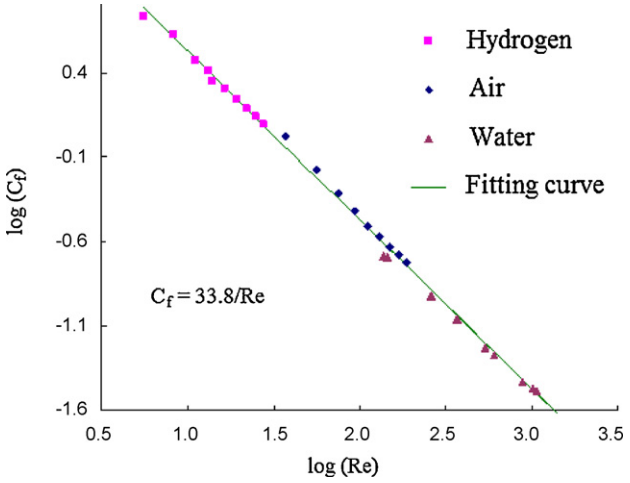

Fig. 5. The relationship between log(C_f) and log(Re) in single-phase flow.

and it is used to calculate the frictional gradient in Appendix A. Next we will focus on the relationship of pressure drop, gas and liquid superficial velocities under the critical condition, when the flow pattern transits from intermittent flow to annular flow.

4.2. Effect of annular purge

The experimental results with predicted critical pressure drops are shown in Fig. 6. The fuel cell was kept at the state of open circuit to eliminate the effects of hydrogen consumption, which will be discussed in Section 4.4. Other operation conditions were as follows: the volume velocity of hydrogen was maintained 96 sccm (thus 1.76 m s^{-1} in the channel), and the cell temperature was controlled to be 50 °C, while the humidifiers were kept at 60 °C. Therefore, when the supersaturated flow went into the cell, it would turn to two phases with tiny condensed water. This would simulate the built-up of water during the operation of a fuel cell and speed up this process. After the pretreatment of signal noise based on wavelet analysis, the pressure changes with the elapsed time are shown as the black curve in Fig. 6. Meanwhile the critical pressure drops are also predicted by the annular purge model (the red curve). Thus, if the experimental pressure drops are higher than the critical values, the annular pure process may happen.

In our experiments, the hydrogen inlet pressure will increase by a back-pressure valve. After closing for a few seconds, open the valve

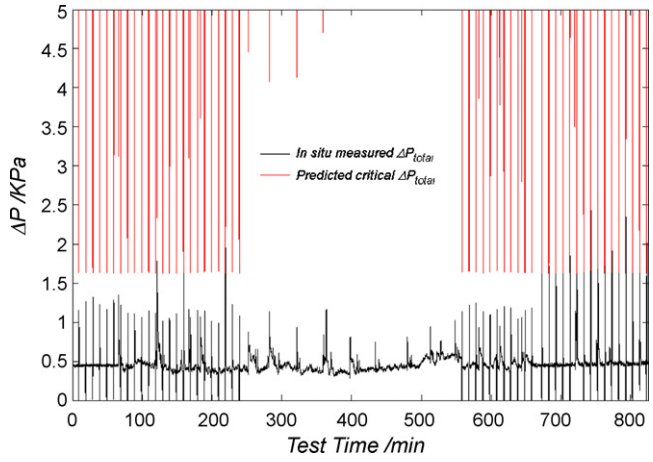

Fig. 6. The effect of purging in different pressure drops.

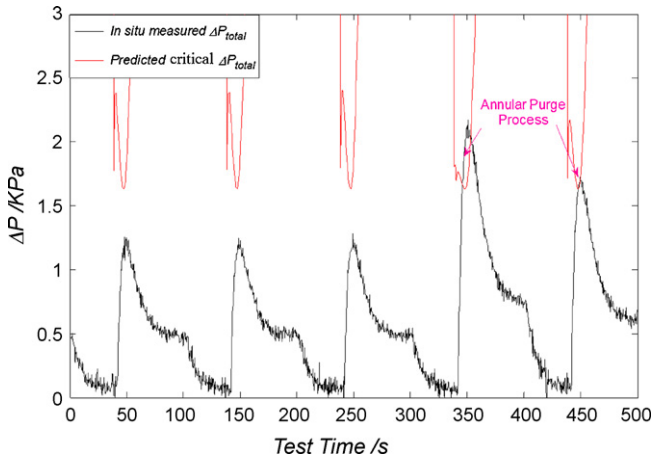

Fig. 7. The predicted area for annular purge process.

and the purge process will happen. By controlling the close time, the pulse flow will be regulated, and the corresponding changes of pressure drops are discussed by stages below:

(1) 0–240 min: close the back-pressure valve for 40 s every 10 min, and most of the responding pressure drops were lower than the critical pressure. The pressure drops would become unstable gradually, which meant more water accumulated in the flow field. During this period, the intermittent purge would happen from time to time.
(2) 240–560 min: open the valve all the time, and the intermittent purge would happen sometimes.
(3) 560–680 min: repeat the same operation as stage 1, it is still unstable.
(4) 680–900 min: close the valve for 60 s every 10 min, and it would make the pressure drop higher than the critical value. Thus, the annular purge might happen. It could remove the liquid water from the channel effectively, because the pressure drops had small fluctuation around 0.45 kPa under the steady operation. However, we have to point out that the intermittent purge may happen during this period, if the average speed of water accumulation is higher than that of water removal.

In short, lots of liquid water will remain in the anode GFC after the intermittent purge process, and it should be avoided; while the annular purge will remove the accumulated water effectively. However, it will not happen until the pressure drops are higher than the critical values (the red line).

4.3. The prediction of the critical pressure drops

The detailed comparison is shown in Fig. 7, and the operation conditions are the same as above. The black curve represents the pressure drops of the channel, which were measured in situ by pressure transducer. By contrast, the red curve represents the corresponding critical pressure drops predicted by our annular purge model, and it has a minimum value. Thus, the intersection of the two curves is the area where the annular purge can happen. In Fig. 7, the first three flow pulses did not reach the critical values, and the accumulated water still attached the GFC surface. However, the annular purge would happen if the pressure drop was higher than the critical value of ΔP_{total} in the forth flow pulse. By comparing the measured pressure drops, we can also deduce that if more liquid water is accumulated, the measured pressure drop will be higher and the gravitation will take more effects.

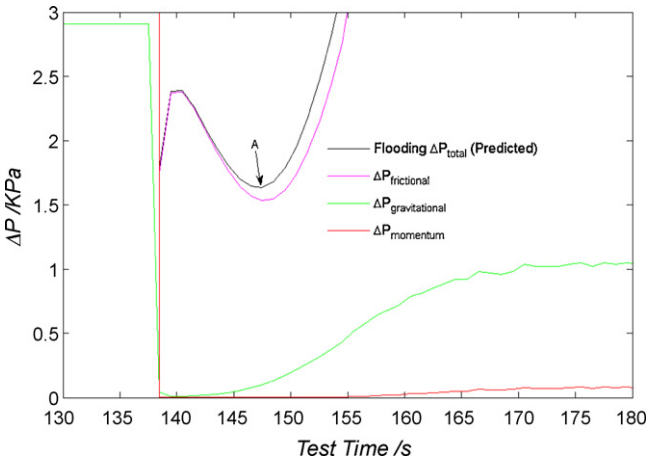

Fig. 8. The composition of the critical pressure drop in a certain pulse flow.

4.4. The proportions of three pressure components

Maintained much the same operation conditions as in Fig. 6, the fuel cell was discharging at 1 A cm^{-2}, and the hydrogen stoichiometric ratio was 3 in the stable flow of 96 sccm. Thus, the momentum change of the two-phase flow has to be considered. Based on the analysis of a pulse flow, the predicted critical pressure drops are shown as the black curve in Fig. 8. It is obvious that the frictional pressure drop is greater than the gravitational and the momentum term. These values are 1.55 kPa, 80 Pa and 0.5 Pa, respectively at point A, which is the minimum critical pressure drop.

5. Conclusions

In this work, a transparent anode separator is used to observe the two-phase flow during the purge process, which is distinguished as the intermittent purge and the annular purge. In the intermittent purge, most of the accumulated water stays at the channel and leads to the unsteady performance of the fuel cell. In the annular purge, however, the liquid phase can be removed from the channel effectively, and the fluctuation of the pressure drops is small in the steady state. The annular purge will not happen until the pressure drop is higher than the critical value, which is predicted by the annular purge model. In addition, the proportions of the frictional, gravitational and momentum term are given under the critical condition, and usually the frictional term is in the majority.

List of symbols

A	cross-section area (m^2)
Bo	Bond number
C	a constant
C_f	friction coefficient
D_e	equivalent diameter (m)
F	wall friction (N)
Fr	Froude number
g	acceleration of gravity (9.81 m s^{-2})
G	mass flux (kg m^{-2} s^{-1})
Ku	Kutateladze number
L	the effect length of the anode channel (m)
m	mass of the body (kg)
M	molar mass (g mol^{-1})
P	pressure (Pa)
Q	volume flow rate (sccm)
Re	Reynolds number
S	slip ratio
t	time (s or min)
u	velocity (m s^{-1})
V	superficial velocity (m s^{-1})
x	quality
z	z direction
Z	distance from the inlet (m)

Greek letters

ρ	density (kg m^{-3})
μ	viscosity (Pa s)
τ	shear stress (N m^{-2})
σ	surface tension (N m^{-1})
α	void fraction
λ	stoichiometric ratio
ε	roughness (m)
θ	static contact angle

Subscripts

l	liquid phase
g	gas phase
w	water (at room temperature)
i	note for species (hydrogen, air or water)
in	inlet of the cell

Appendix A. Algorithm for calculation of critical pressure drop for the annular purge process

Step 1: Measure the flow rate of hydrogen (Q_g), then the superficial velocity of the gas can be calculated:

$$V_g = \frac{Q_g}{A} \tag{A.1}$$

Step 2: Calculate the liquid superficial velocity under the critical condition:

$$\mathrm{Ku} = \frac{V_g \rho_g^{1/2}}{[g\sigma(\rho_l - \rho_g)]^{1/4}} \tag{A.2}$$

$$\mathrm{Bo} = \frac{D_e^2 g(\rho_l - \rho_g)}{\sigma} \tag{A.3}$$

$$\mathrm{Fr}^{0.22} = 0.286\ \mathrm{Bo}^{0.26}\left[1 + \frac{\mu_l}{\mu_w}\right]^{-0.18} K_g^{-1} \tag{A.4}$$

$$V_l = \frac{4}{\pi}\left[\frac{\sigma}{g(\rho_l - \rho_g)}\right]^{1/4} \mathrm{Fr} \tag{A.5}$$

Step 3: Calculate the two-phase flow parameters:

$$G_g = \rho_g V_g \tag{A.6}$$

$$G_l = \rho_l V_l \tag{A.7}$$

$$G_{total} = G_g + G_l \tag{A.8}$$

$$x = \frac{G_g}{G_{total}} \tag{A.9}$$

$$S = \left[1 - x\left(1 - \frac{\rho_l}{\rho_g}\right)\right]^{1/2} \tag{A.10}$$

$$\alpha = \left[1 + \left(S\frac{1-x}{x}\frac{\rho_g}{\rho_l}\right)\right]^{-1} \tag{A.11}$$

Step 4: Calculate the frictional coefficient:

$$Re = \frac{G_i D_e}{\alpha_i \mu_i} \tag{A.12}$$

$$C_f = \frac{33.8}{\mathrm{Re}} \tag{A.13}$$

Step 5: Calculate the frictional gradient:

$$\left(-\frac{dP}{dz}\right)_{\text{frictional}} = \left(-\frac{dP}{dz}\right)_{l} + C\left[\left(-\frac{dP}{dz}\right)_{l}\left(-\frac{dP}{dz}\right)_{g}\right]^{1/2} + \left(-\frac{dP}{dz}\right)_{g} \quad (A.14)$$

$$-\left(\frac{dP}{dz}\right)_{g} = \frac{4C_f}{D_e}\frac{{G_g}^2}{2\rho_g} \quad (A.15)$$

$$-\left(\frac{dP}{dz}\right)_{l} = \frac{4C_f}{D_e}\frac{G_l^2}{2\rho_l} \quad (A.16)$$

$$\Delta P_{\text{frictional}} = -\left(\frac{dP}{dz}\right)_{\text{frictional}} \times L \quad (A.17)$$

Step 6: Calculate the gravitational gradient:

$$-\left(\frac{dP}{dz}\right)_{\text{gravity}} = [\alpha\rho_g + (1-\alpha)\rho_l]g \ \sin\Theta \quad (A.18)$$

$$\Delta P_{\text{gravity}} = -\left(\frac{dP}{dz}\right)_{\text{gravity}} \times L \quad (A.19)$$

Step 7: Calculate the momentum gradient:

$$G_g(Z) = \left(1 - \frac{1}{\lambda}\frac{Z}{L}\right)G_g \quad (A.20)$$

$$G_l(Z) = G_l + \frac{M_l}{M_g}\frac{\text{Pw}}{P-\text{Pw}}(G_g - G_g(Z)) \quad (A.21)$$

$$G_{\text{total}}(Z) = G_l(Z) + G_g(Z) \quad (A.22)$$

$$x(Z) = \frac{G_l(Z)}{G_{\text{total}}(Z)} \quad (A.23)$$

$$S = \left[1 - x(Z)\left(1 - \frac{\rho_l}{\rho_g}\right)\right]^{1/2} \quad (A.24)$$

$$\alpha(Z) = \left[1 + \left(S(Z)\frac{1-x(Z)}{x(Z)}\frac{\rho_g}{\rho_l}\right)\right]^{-1} \quad (A.25)$$

$$\Delta P_{\text{momentum}} = \left[G_{\text{total}}(z)^2\left(\frac{x(z)^2}{\alpha(z)\rho_g} + \frac{(1-x(z))^2}{(1-\alpha(z))\rho_l}\right)\right]_0^L \quad (A.26)$$

Step 8: Calculate the total pressure drop under the critical condition:

$$\Delta P_{\text{total}} = \Delta P_{\text{frictional}} + \Delta P_{\text{gravitational}} + \Delta P_{\text{momentum}} \quad (A.27)$$

Step 9: Criterion:If $(\Delta P_{\text{total}})_{\text{measured}} \geq (\Delta P_{\text{total}})_{\text{critical}}$, the annular purge process may happen.

References

[1] Y. Baolian, Fuel Cell—Principle, Technology and Application, Chemical Industry Press (CIP), Beijing (2003.7), 160.
[2] A. Kraytsberg, Y. Ein-Eli, Journal of Power Sources 160 (2006) 194–201.
[3] W.M. Yan, F.L. Chen, H.Y. Wu, C.Y. Soong, H.S. Chu, Journal of Power Sources 129 (2004) 127–137.
[4] S. Ge, C.Y. Wang, Journal of the Electrochemical Society 154 (2007) B998–B1005.
[5] J. Yuan, B. Sunden, M. Hou, H. Zhang, Numerical Heat Transfer. Part A: Applications 46 (2004) 669–694.
[6] Y. Wang, S. Basu, C.-Y. Wang, Journal of Power Sources 179 (2008) 603–617.
[7] S. Waelchli, P.R. von Rohr, International Journal of Multiphase Flow 32 (2006) 791–806.
[8] V.G. Nino, E.W. Jassim, P.S. Hrnjak, T.A. Newell, Hvac&R Research 12 (2006) 17–34.
[9] Z. Bilicki, J. Kestin, J. Mikielewicz, International Journal of Heat and Mass Transfer 30 (1987) 1427–1434.
[10] W.L. Chen, M.C. Twu, C. Pan, International Journal of Multiphase Flow 28 (2002) 1235–1247.
[11] P. Changhong, G. Yun, Q. Suizheng, J. Dounan, N. Changhua, Nuclear Engineering and Design 235 (2005) 1737–1747.
[12] X. Yu, M. Pinwen, H. Ming, Y. Fu, B. Yi, Z.-G. Shao, Journal of Power Sources 185 (2008) 1009–1014.
[13] Y.H. Cai, J. Hu, H.P. Ma, B.L. Yi, H.M. Zhang, Journal of Power Sources 161 (2006) 843–848.
[14] G.B. Wallis, AEEW-R123 (1961).
[15] O.L. Pushkina, Y.L. Sorokin, Heat Transfer Soviet Research 1 (1969) 56–64.
[16] K.W. McQuillan, P.B. Whalley, G.F. Hewitt, International Journal of Multiphase Flow 11 (1985) 741–760.
[17] P.B. Whalley, Boiling, Condensation, and Gas–Liquid Flow, Oxford University Press, New York, Toronto, 1987.
[18] D. Chisholm, NEL Report (1972) 535.
[19] J. Yue, G.W. Chen, Q. Yuan, Chemical Engineering Journal 102 (2004) 11–24.